ELECTRONIC SUPPLEMENTARY INFORMATION

Non-ionic hydrophobic eutectics - versatile solvents for tailored metal separation and valorisation

Nicolas Schaeffer[†*], João H.F. Conceição[†], Mónia A. R. Martins[†], Márcia C. Neves[†], Germán Pérez-Sánchez[†], José R.B. Gomes[†], Nicolas Papaiconomou[‡], João A.P. Coutinho[†*]

[†] *CICECO, Aveiro Institute of Materials, Department of Chemistry, University of Aveiro, Campus Universitário de Santiago, 3810-193 Aveiro, Portugal.*

[‡] *Université Nice Sophia Antipolis, Department of Chemistry, 28 Avenue Valrose, 06103 Nice, France*

* Corresponding authors: nicolas.schaeffer@ua.pt; jcoutinho@ua.pt

Number of pages: 30

Number of Figures: 18

Number of Tables: 9

Experimental Section

Chemicals and Instrumentation

Information on the HES constituents used, including their chemical supplier, purity, melting properties, stereochemistry, water solubility and chemical structure is available in **Table S2** and **Figure S1**. The salts $CoCl_2.6H_2O$ (99% purity), $FeCl_3.6H_2O$ (99% purity) and $CrCl_3.6H_2O$ (99% purity) were purchased from Merck, $NiCl_2.6H_2O$ (97% purity) and $CoCl_2.2H_2O$ (98% purity) from BDH Chemicals, $Cu(CH_3COO)_2.H_2O$ (99% purity), NaCl (99.5% purity), NaOH (99% purity) and $NaClO_4$ (98% purity) from Panreac, $PdCl_2$ (99% purity) from SigmaAldrich and $PtCl_4$ (99% purity) from Acros Organics. Hydrochloric acid (37%) was obtained from Fisher Scientific and thiourea (99% purity) from Acros Organic. Ultrapure water, which was double distilled, passed by a reverse osmosis system and further treated with a Milli-Q plus 185 water purification apparatus was used in all experiments.

All eutectic mixtures were prepared by mass using an analytic balance Mettler Toledo XP205 (precision = 0.2 mg). The thermal events of the pure compounds and their mixtures were obtained using a Hitachi DSC7000X working at atmospheric pressure. The equipment was previously calibrated with several standards with mass fraction purities higher than 99%. At least three cycles were performed for the pure compounds and one for the mixtures. Cooling and heating cycles were performed at 5 K.min^{-1} and 2 K.min^{-1}, respectively. Thermal transitions were taken as the peak temperature. In specific cases the melting temperature of powdered solid mixtures was determined with an automatic glass capillary device model M-565 from Buchi, with a temperature resolution of 0.1 K, at 0.1 K.min^{-1}. Densities and viscosities were measured at atmospheric pressure and at different temperatures using a SVM 3001 Anton Paar viscometer (reproducibility: temperature 0.03 K; density 0.0001 g.cm^{-3}; viscosity 0.35%). The water content of the pure compounds and their eutectic mixtures at room temperature was evaluated using a Metrohm 831 Karl Fischer coulometer with Hydranal®-Coulomat AG from Riedel-de Haën. ^{1}H-, ^{12}C- and ^{31}P-Nuclear Magnetic Resonance (NMR) analysis was performed using a Bruker Avance 300 operating at 75 MHz using deuterated water (D_2O) placed in a coaxial insert as solvent. In some cases, the water peak was suppressed using the Bruker NMR software. The morphology of the palladium nanoparticles obtained during the stripping stage was observed using a Hitachi HD-2300 Scanning Transmission Electron Microscope (TEM) and the particle size analysed using the ImageJ software package.

Metal concentration in the aqueous phase was determined by UV-Vis analysis in the range of 200−850 nm using a Shimadzu PharmaSpec UV-1700 spectrophotometer with a quartz cuvette. For each metal, two calibration curves at 0.05 M HCl and 2 M HCl were determined using five different metal concentrations and the samples appropriately diluted to match either HCl concentration. The wavelength employed for each metal determination is listed in **Table S3**. All calibration curves were obtained with an $R^2 \geq 0.99$. Depending on the absorptivity of the metal complexes different path lengths were employed; a quartz cuvette with a 20 mm path length was used for the determination of Cu, Co, Ni and Cr concentrations whilst a quartz cuvette with a 1 mm path length was used for the determination of Pt, Pd and Fe concentrations. Due to potential interferences stemming from transfer of the aromatic HES component to the aqueous phase during extraction (especially for wavelengths below 300 nm), for each extraction condition an identical system without metal was used as a baseline.

Screening of hydrophobic eutectic mixtures

A total of 15 compounds were selected as potential HES constituents based on (i) previously reported DES and (ii) their melting temperature and melting enthalpies (**Table S2**). Selected compounds include terpenes (thymol and eugenol), bio-derived carboxylic acids (capric acid, salicylic acid, vanillic acid, syringic acid, trans-ferrulic acid, hydrocinnamic acid, mandelic acid), acetylsalicylic acid, caffeine, coumarin and TOPO. Three molar ratios of 1:3, 1:1 and 3:1 were arbitrarily selected for each mixture to rapidly probe the potential to form liquid HES at room temperature. However, only the molar ratio closest to the predicted ideal eutectic composition based on the ideal solubility curves of the potential mixtures obtained using Equation (1) were experimentally attempted to reduce the total number of initial tests. Each mixture was prepared by careful weighting of the components (total mass 1 g) followed by heating at 373 K under agitation for 1 hr and left to cool overnight at room temperature. Samples that solidified or displayed visible signs of degradation (marked change in colour) were omitted. From the initial HES 132 combinations tested, 14 new mixtures were identified as liquid HES at 298 K; these systems are listed in **Table S4**. The obtained HES were visually screened for their stability in the acidic environment typically encountered in solvent extraction processes. A fixed volume of HES (1 mL) was contacted with an equivalent volume of 1 M HCl solution for 24 hr at room temperature. With the exception of eugenol-based HES that displayed a progressive darkening with time, all other HES were stable at this acidic pH (pH=0).

Characterisation of selected HES

Three systems were elected for further study: Thymol+TOPO (Th+TOPO), TOPO+Capric acid (TOPO+CA) and Hydrocinnamic acid+Capric acid (HA+CA). The phase diagram of each HES was determined by preparing binary mixtures in different proportions covering the full composition range (at 0.1 mole fraction intervals). Samples were heated under stirring at a temperature 10 K above the melting temperature of the pure compound with the highest melting point, until a homogenous liquid was formed and then stirred in the liquid state for more 30 minutes. After cooling at room temperature samples of 2-5 mg were: i) hermetically sealed in aluminum pans and weighed in a micro-analytical balance AD6 (PerkinElmer, precision = 0.002 mg) or ii) placed in glass capillaries. To further characterize the Th+TOPO, TOPO+CA and HA+CA systems, one mixture per system with equimolar composition (1:1) was prepared in a larger quantity following the procedure above. These were analysed by NMR and their water content, viscosity and density measured. Additionally, the influence of water and 1 M HCl on the HES phase as well as the potential loss of the HES component to the aqueous phase was followed by ^{1}H-NMR.

Thermodynamic modelling of the Solid-Liquid Equilibria (SLE)

The phase equilibria of the eutectic mixtures with complete immiscibility in the solid phase can be described by Equation (S1):

$$ln\left(x_i y_i^l\right) = \frac{\Delta H_m}{R}\left(\frac{1}{T_m} - \frac{1}{T}\right)$$

(S1)

where x_i is the mole fraction solubility of compound i and γ_i^l its activity coefficient in the liquid phase, T is the absolute temperature, T_m and ΔH_m are the melting temperature and enthalpy of the pure solute, respectively, and R is the universal gas constant.[1-2] Equation (S1) is a simplified version of the solid-liquid equation, where the term related with heat capacities is neglected due to its small contribution to the phase equilibrium calculations.[2,3] This assumption is reasonable based on the small temperature difference between the eutectic and the melting temperature of the pure compounds (TOPO, thymol, capric acid and hydrocinnamic acid). Under such conditions, previous work showed that omission of even large $\Delta_m C_p$ values resulted in errors of only 0.5 K or less in the phase diagram.[3] When ideality is assumed, γ_i^l equals 1 and the solubility curves are derived from Equation (S1). The

experimental activity coefficients can also be obtained through Equation (S1) using the experimental data.

Metal extraction in selected HES

The partition of the chloride salts of Pt^{4+}, Pd^{2+}, Cr^{3+}, Fe^{3+}, Cu^{2+}, Co^{2+} and Ni^{2+} in the three HES Th+TOPO, TOPO+CA and HA+CA was initially assessed at three different HCl concentrations of 0 M HCl (0.05 M HCl for Pt^{4+} and Pd^{2+} to prevent hydrolysis), 1 M HCl and 2 M HCl. The concentration of Pt^{4+} and Pd^{2+} was 2 mM whilst that of Cr^{3+}, Fe^{3+}, Cu^{2+}, Co^{2+} and Ni^{2+} was 10 mM. All extraction tests were performed using single element solutions, an organic to aqueous volumetric phase ratio (O:A) of 0.5 and a 1:1 HES molar composition. The extraction of Pd^{2+} in the Th+TOPO HES was further investigated as function of multiple factors including HCl concentration (0.1 to 4 M HCl), Pd^{2+} concentration (0.5 to 20 mM) and TOPO molar fraction (0.2 to 0.5) at room temperature and O:A=0.5 (total volume 1.5 mL). Unless otherwise specified standard conditions of 10 mM $PdCl_2$ concentration, 2 M HCl and a TOPO molar fraction (x_{TOPO}) of 0.5 were applied. For all metal extractions, samples were mixed under constant agitation (1000 rpm) and temperature (298 K) for 5 min using an Eppendorf Thermomixer Comfort equipment. Following extraction, samples were centrifuged for 5 min at 5000 rpm and the phases separated. Metal concentration in the aqueous phase was measured by UV-vis analysis following appropriate dilution. Metal ion (M^{n+}) distribution coefficients (D_M) and the separation factor between two given metals ($\alpha_{M1/M2}$) are calculated using Equations (S2) and (S3).

$$D_M = \frac{[M]_{HES,f}}{[M]_{aq,f}} = \frac{([M]_{aq,in} - [M]_{aq,f})}{[M]_{aq,f}} \times \frac{V_{aq}}{V_{HES}}$$

(S2)

$$\alpha_{M1/M2} = \frac{D_{M1}}{D_{M2}}$$

(S3)

where the subscript HES and aq denote the phase and *in* and *f* the time frame (*in* – before extraction and *f*– after extraction). Due to the negligible mutual solubilities during extraction, the phase volume ratio remained practically unchanged after extraction. All tests were performed in triplicate with the average value reported.

Palladium recovery from the Th+TOPO phase

Stripping of the Th+TOPO HES phase after extraction of 10 mM Pd^{2+} from a 1 M HCl solution (extraction conditions: O:A=0.5, x_{TOPO}=0.5) was performed using a 0.1 M thiourea in 0.5 M HCl solution, an O:A ratio of 0.25 and a mixing time of 0.5 hr at 298 K and 1000 rpm. The stripping percentage (%S) in the stripping phase was determined according to Equation (S4) and represents the amount of Pd^{2+} removed from the organic phase to the total amount of metal in the initial HES phase before stripping ($[M]_{HES,i}$). Following stripping, the recovered HES phase was collected and analysed by NMR to verify its chemical and compositional integrity.

$$\%S_M = \frac{([M]_{HES,in} - [M]_{HES,f})}{[M]_{HES,in}} \times 100$$

(S4)

Alternatively, the same Th+TOPO loaded phase was isolated and vigorously mixed for 5 min with a 0.1 M $NaCH_3COO$ aqueous solution (O:A=0.5) and left to stand at room temperature. A progressive browning of the aqueous phase was observed with time. After three days standing, the aqueous phase was collected and analysed by TEM.

Computer simulations

Molecular dynamics (MD) simulations were carried out using Gromacs 5.1 package[4] within the NpT ensemble by adopting the leapfrog algorithm to integrate the equations of motion at a fixed temperature (298 K) and pressure (1 bar).[5] The OPLS all-atom force field was used for TOPO, thymol and capric acid. Water molecules were represented by the SPC/E model.[6] The potential energy function comprised bond stretching, angle bending, and dihedral torsion terms for bonded interactions. The Lennard-Jones (LJ) potential and the Coulomb term were considered for non-bonded interactions. Hydrogen bonds were constrained by the LINCS algorithm[7] whilst LJ and Coulombic interactions were computed up to a cut-off radius of 1.2 nm. The force-switch van der Waals potential modifier was employed for LJ, where the energy decays smoothly to zero between 0.9–1.2 nm, long-range Coulombic interactions were evaluated by particle mesh Ewald (PME).[8] All simulations were started from a randomly distributed configuration, and production runs were carried for 100 ns with a time step of 2 fs following an energy minimization step using the steepest descent algorithm and two short equilibrium runs in the NVT and NpT ensembles, respectively. The temperature and pressure were controlled through the Nose–Hoover thermostat[9] and the Parrinello–Rahman barostat,[10] respectively. A summary of simulation conditions including system size

and box type are presented in **Table S5** of the supplementary information. MD simulation outputs were visualized using the VMD software package.[11] Radial distribution functions (RDFs) and coordination numbers (CNs) were calculated using Gromacs inbuilt analysis tools.

Density functional theory (DFT) calculations were performed using the Gaussian09 program[12] employing the M06-2X hybrid functional.[13] All HES structures were first pre-optimised at the M06-2X/6-31G level of theory to explore the configurational space starting from two different initial geometries, with both resulting in a similar final arrangement privileging hydrogen bonding. The lowest energy conformer was subsequently optimised at the M06-2X/6-311++G(d,p) level using the Counterpoise keyword to obtain Counterpoise corrected association energies.[14] Optimised structures at the M06-2X/6-311++G(d,p) level were confirmed as true minima on the potential energy surfaces by the absence of imaginary vibrational modes obtained from frequency analysis.

Figures

Acetylsalicylic acid

Caffeine

Coumarin

Capric acid

Hydrocinnamic acid

Thymol

Eugenol

Trioctylphosphine oxide
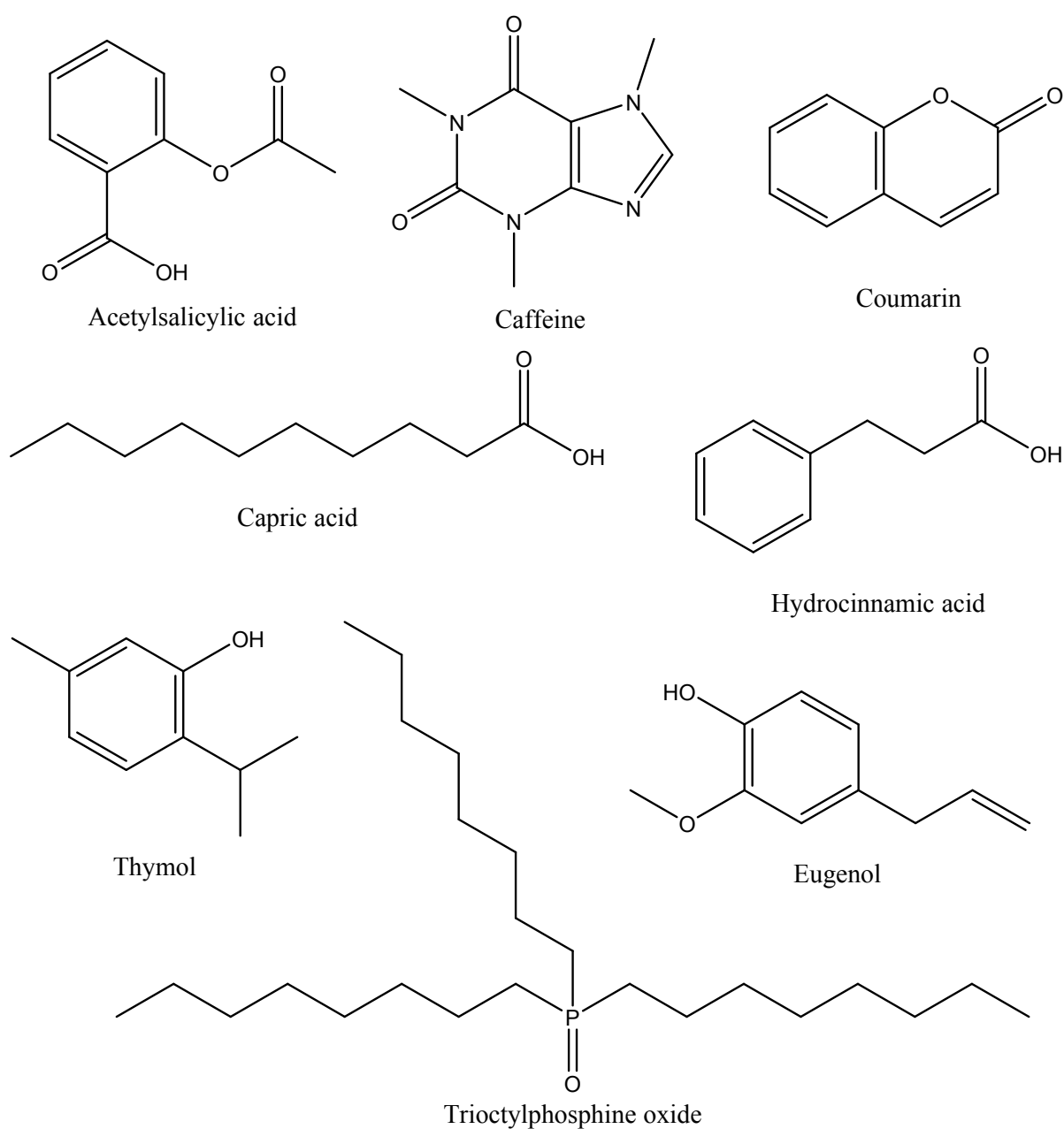
Figure S1. Chemical structures of the compounds used to prepare the eutectic mixtures.
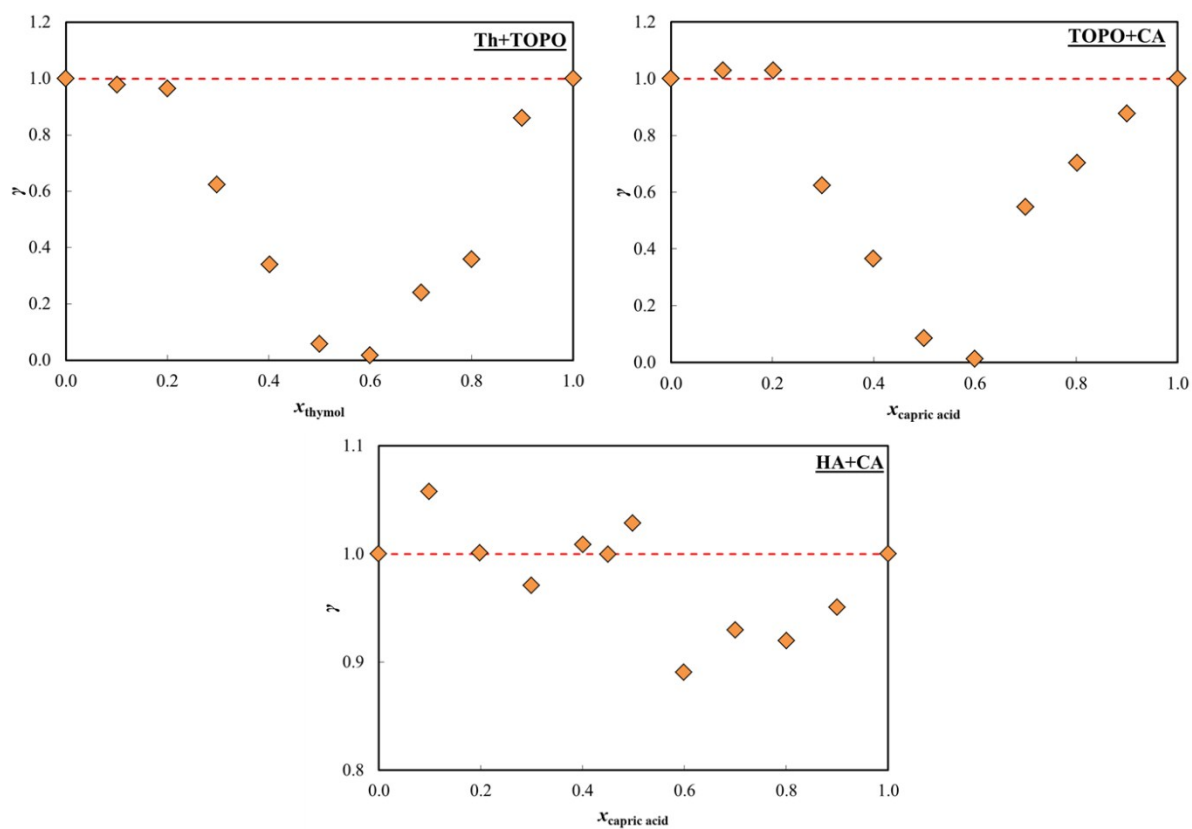
Figure S2. Activity coefficients of the investigated mixtures. Symbols correspond to experimental points and red dotted lines correspond to ideality.
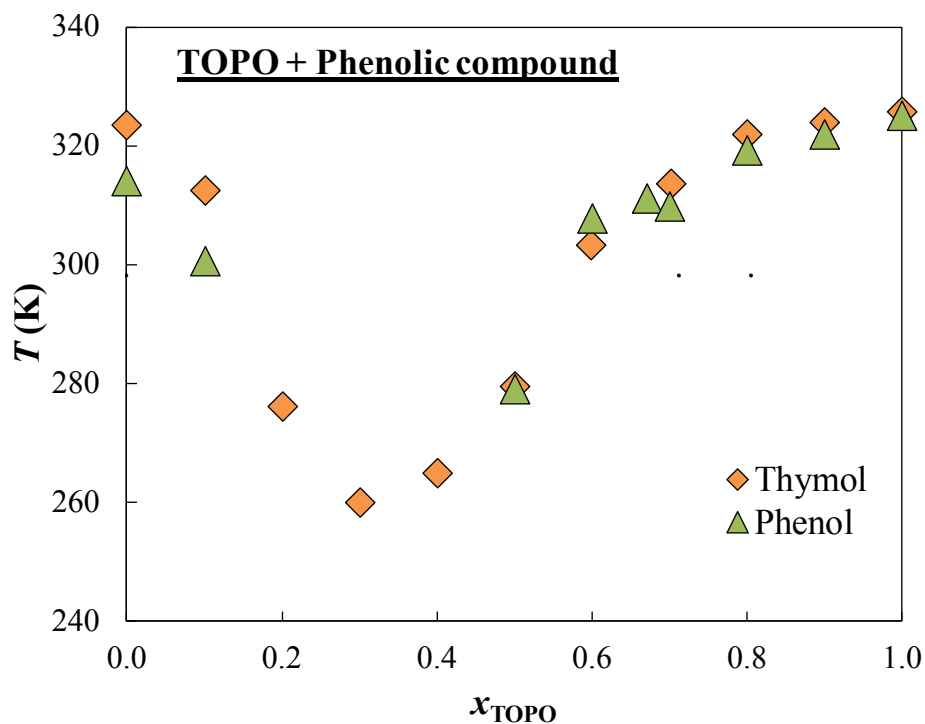
Figure S3. Comparison of the phase diagram of Thymol+TOPO (orange, this work) with Phenol+TOPO (green, ref. 15). Dashed line indicates $T = 298.15$ K.
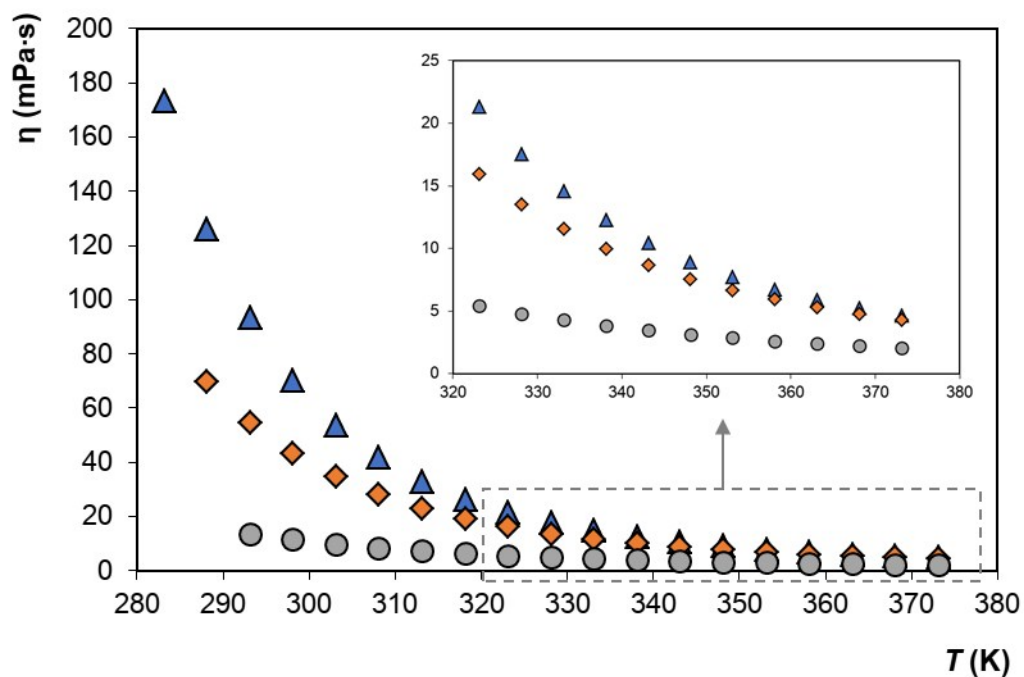
Figure S4. Viscosity of the eutectic mixtures Th+TOPO (▲); TOPO+CA (◆) and HA+CA (●) as a function of temperature (mixture molar ratio of 1:1).
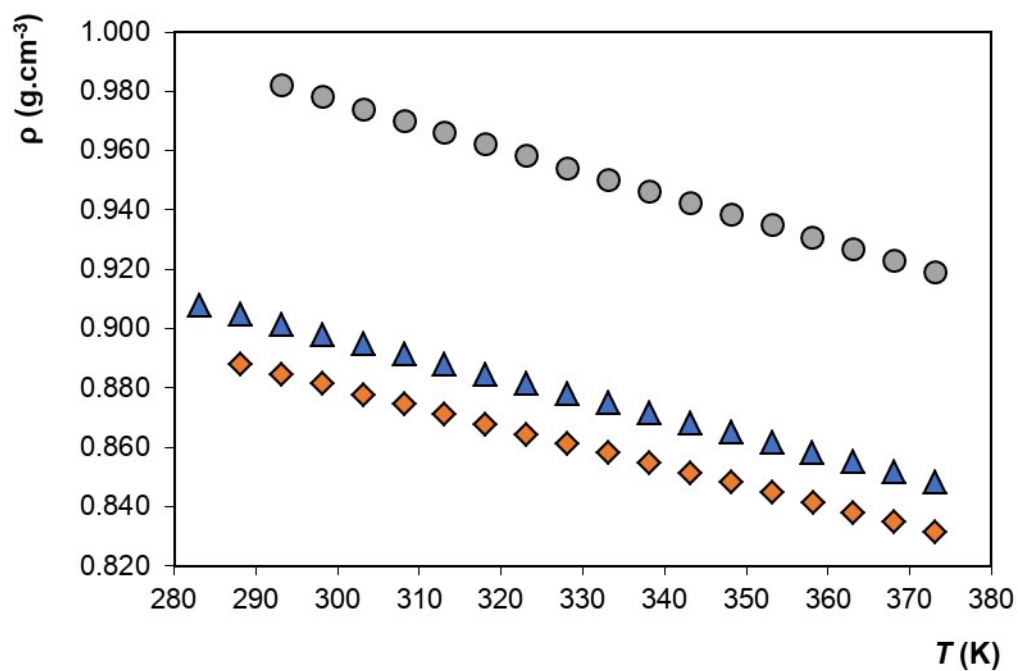
Figure S5. Density of the eutectic mixtures Th+TOPO (▲);TOPO+CA (◆) and HA+CA (●) as a function of temperature (mixture molar ratio of 1:1).
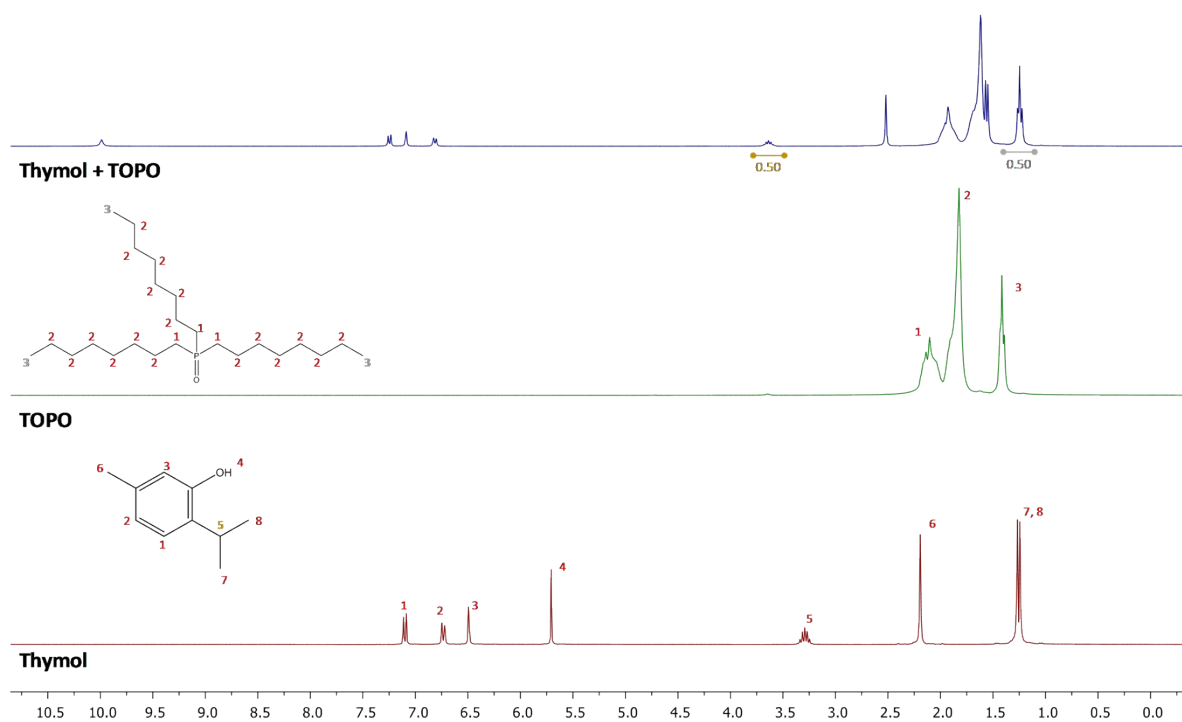
Figure S6. ^{1}H RMN spectra of thymol, TOPO and Thymol + TOPO (1:1) at $T = 323$ K (pure TOPO – 328 K).
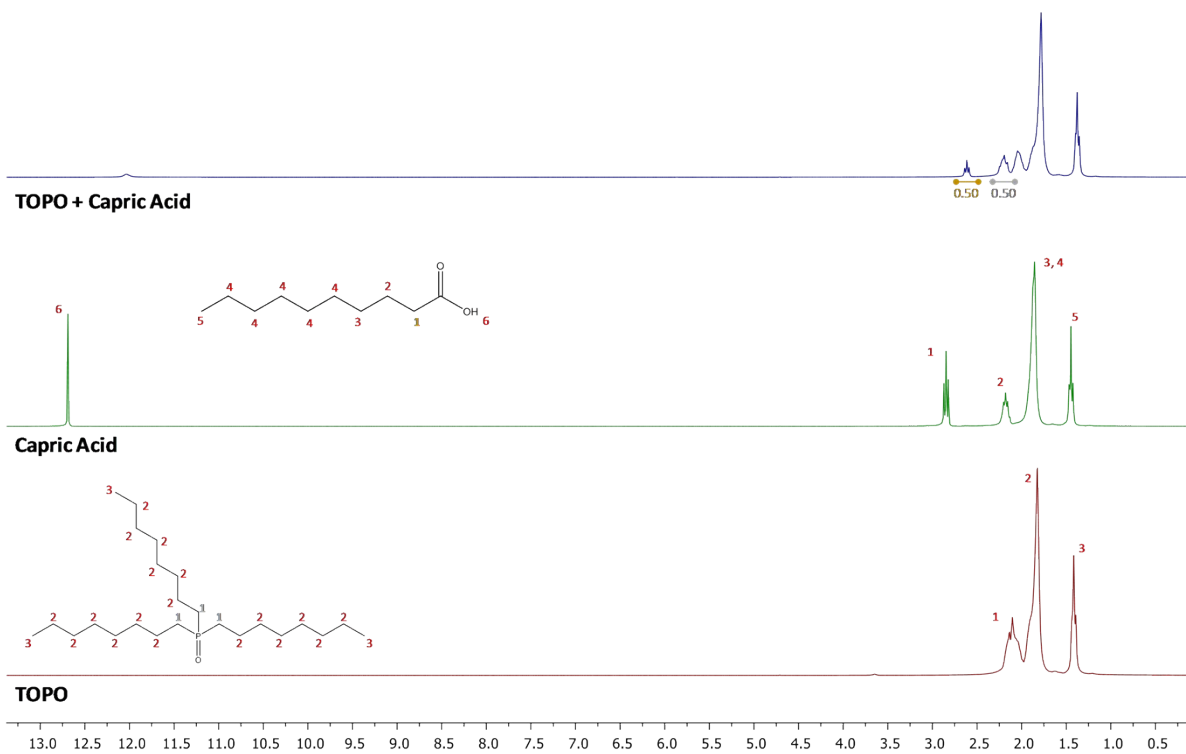
Figure S7. ^{1}H RMN spectra of TOPO, capric acid and TOPO + Capric acid (1:1) at $T = 323$ K (pure TOPO – 328 K).
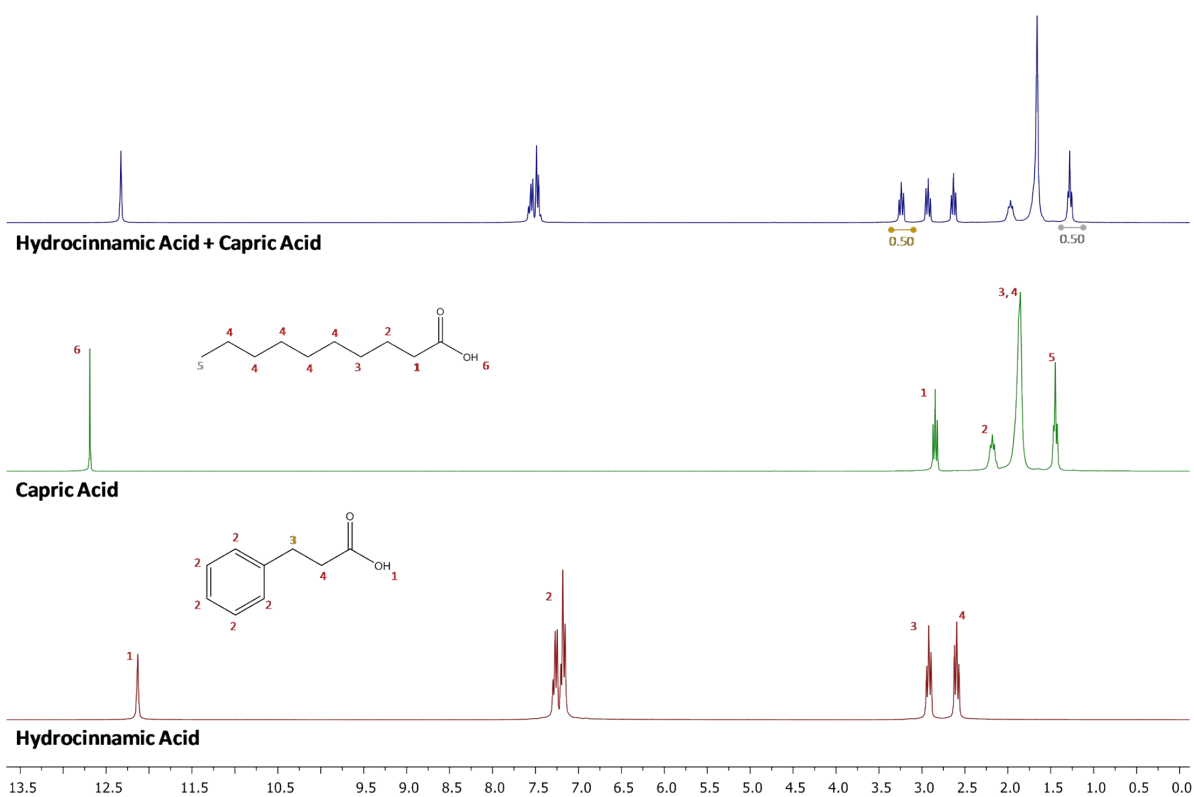
Figure S8. ^{1}H RMN spectra of hydrocinnamic acid, capric acid and Hydrocinnamic acid + Capric acid (1:1) at $T = 323$ K.
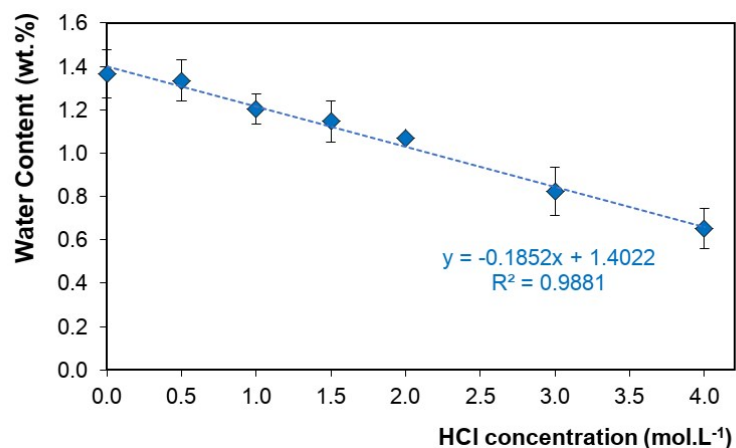
Figure S9. Water content in the Th+TOPO eutectic phase as a function of initial HCl concentration.
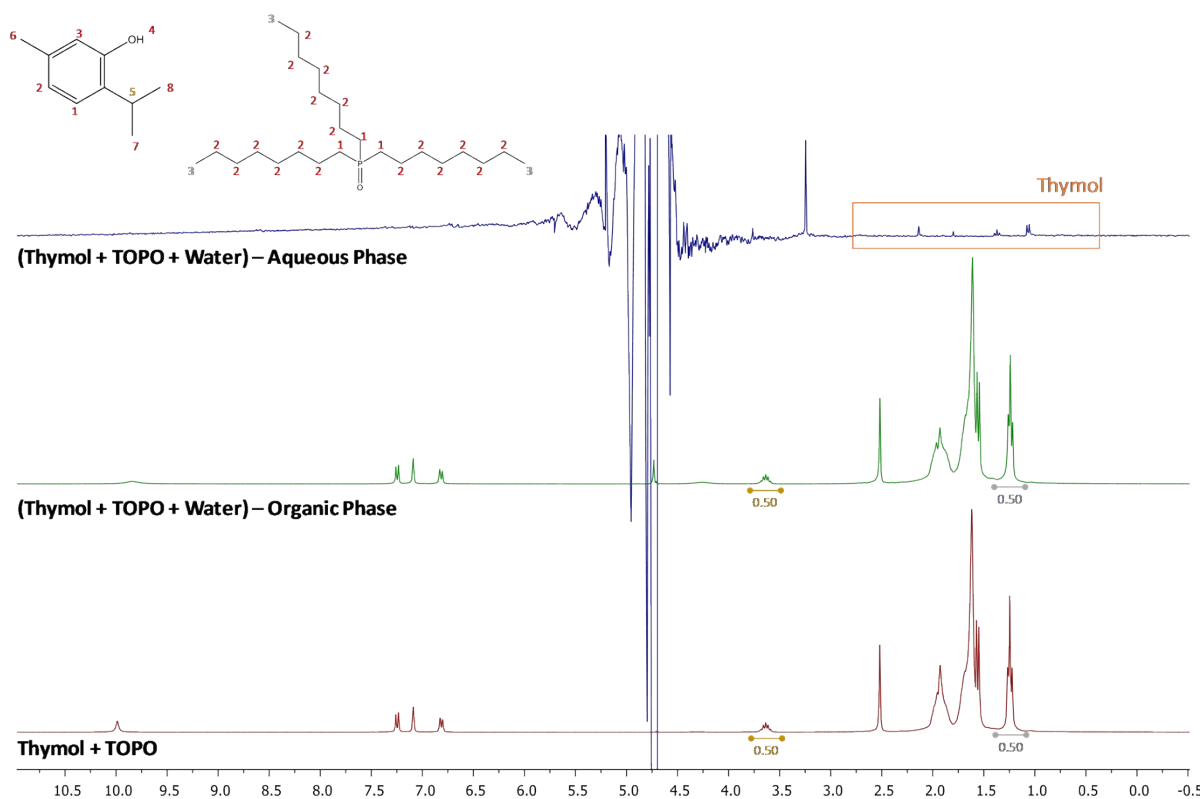
Figure S10. ^{1}H NMR spectra of Thymol + TOPO mixture (1:1) before and after contacting with deionized water for 24 hr at $T = 298$ K as well as the spectra of the aqueous phase after contact. All spectra were recorded at $T = 323$ K.

13
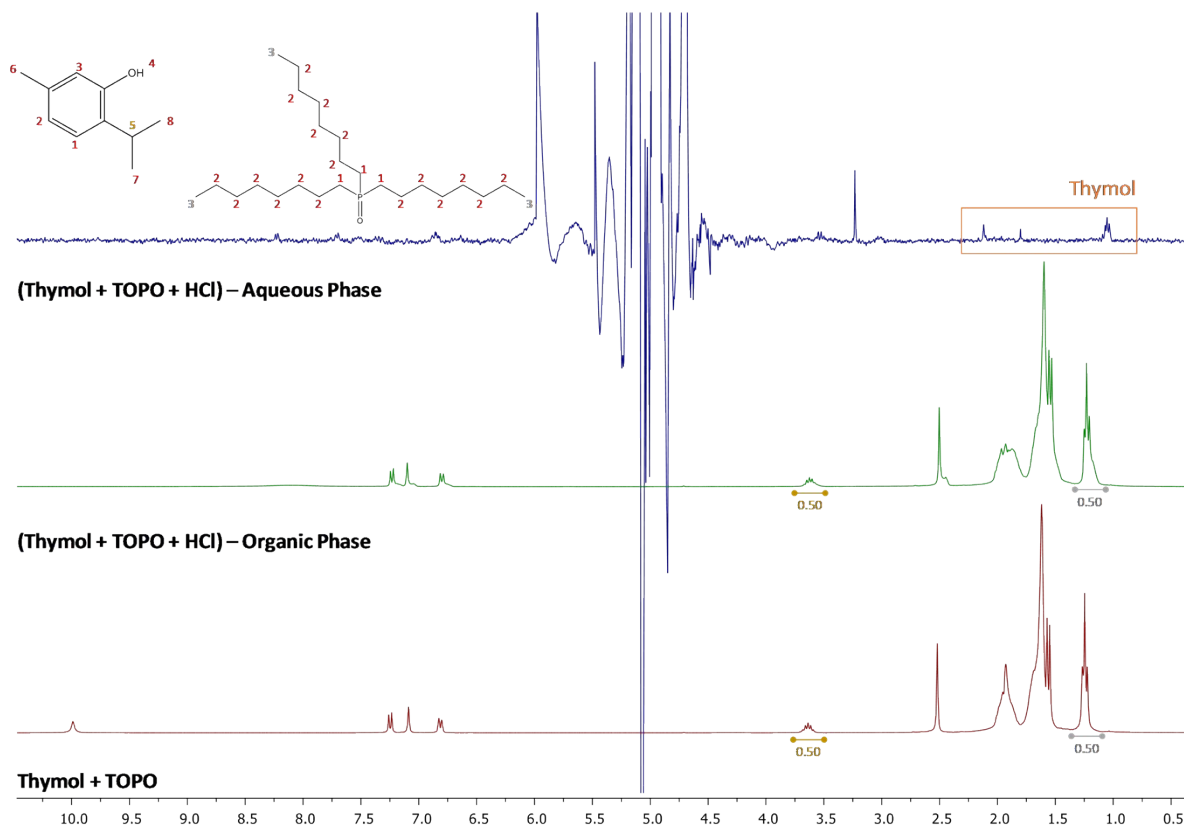
Figure S11. ¹H NMR spectra of Thymol + TOPO mixture (1:1) before and after contacting with an aqueous solution of 1 M HCl for 24 hr at $T = 298$ K as well as the spectra of the aqueous phase after contact. All spectra were recorded at $T = 323$ K.
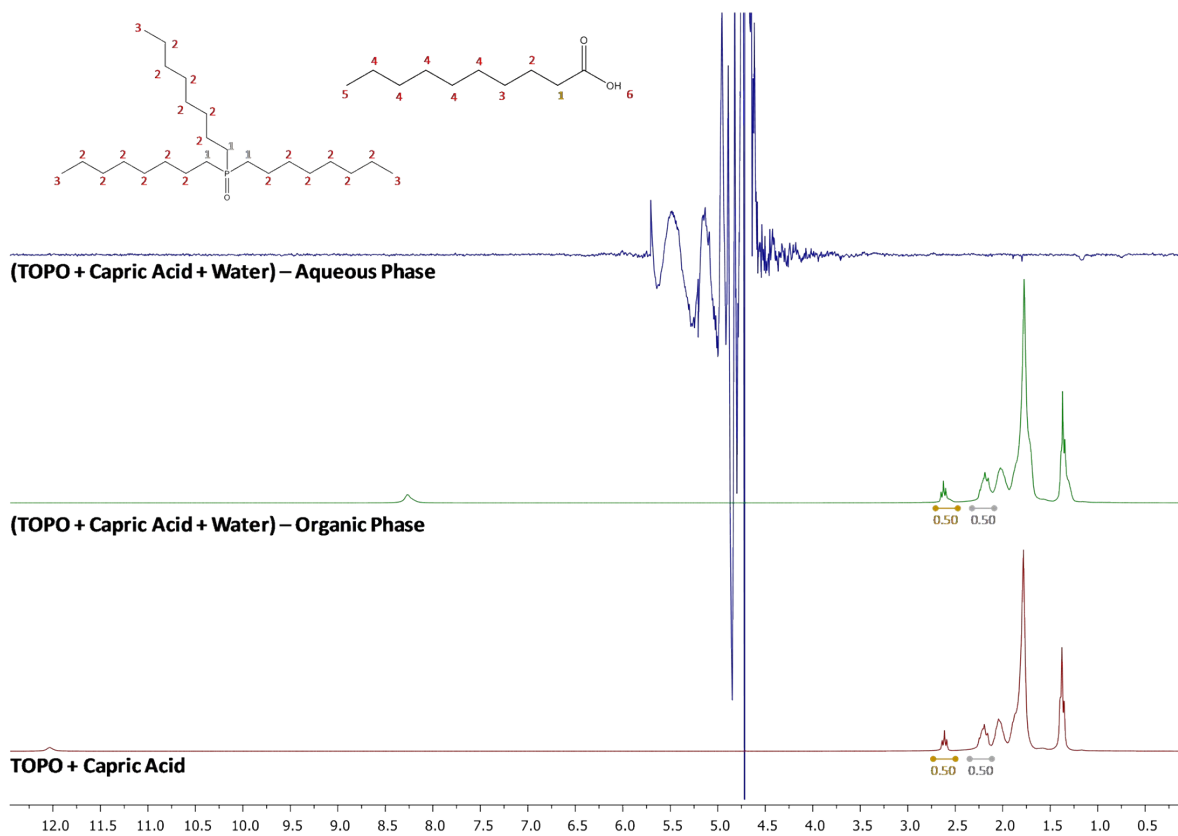
Figure S12. ^{1}H NMR spectra of TOPO+CA mixture (1:1) before and after contacting with deionized water for 24 hr at $T = 298$ K as well as the spectra of the aqueous phase after contact. All spectra were recorded at $T = 323$ K.
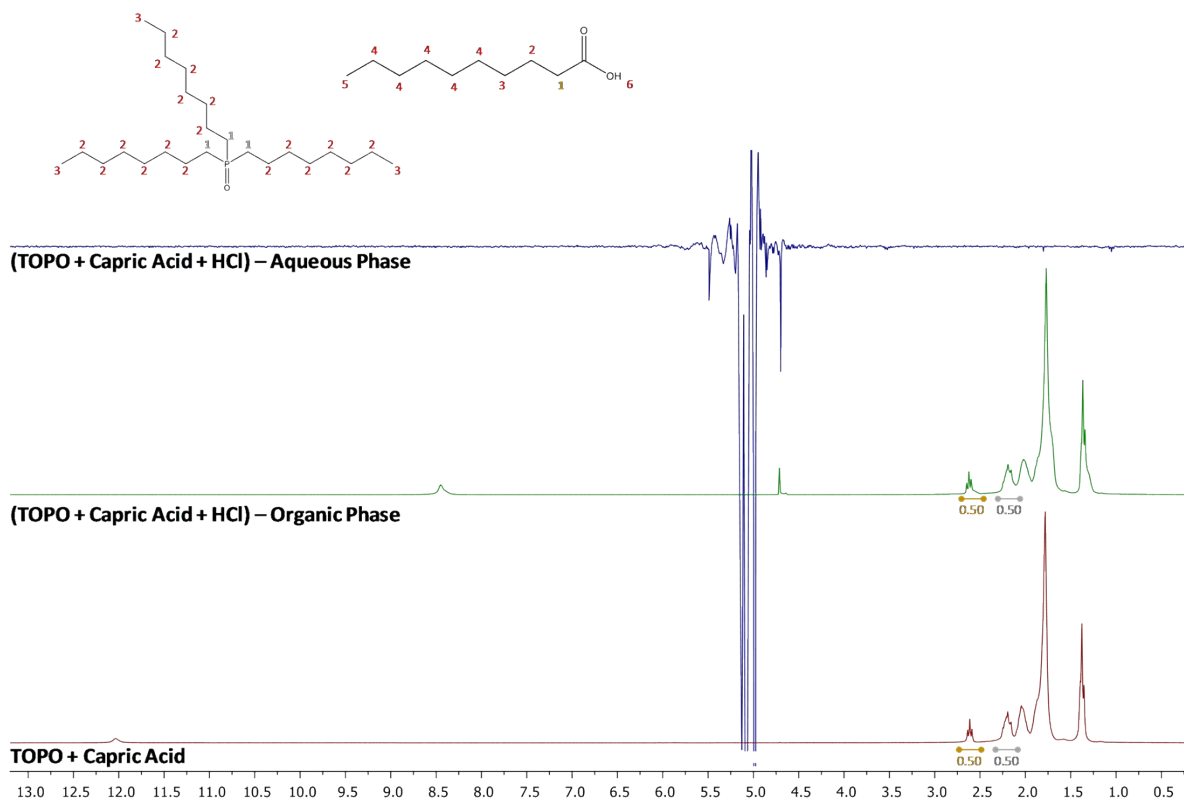
Figure S13. ^{1}H NMR spectra of TOPO+CA mixture (1:1) before and after contacting with an aqueous solution of 1 M HCl for 24 hr at $T = 298$ K as well as the spectra of the aqueous phase after contact. All spectra were recorded at $T = 323$ K.
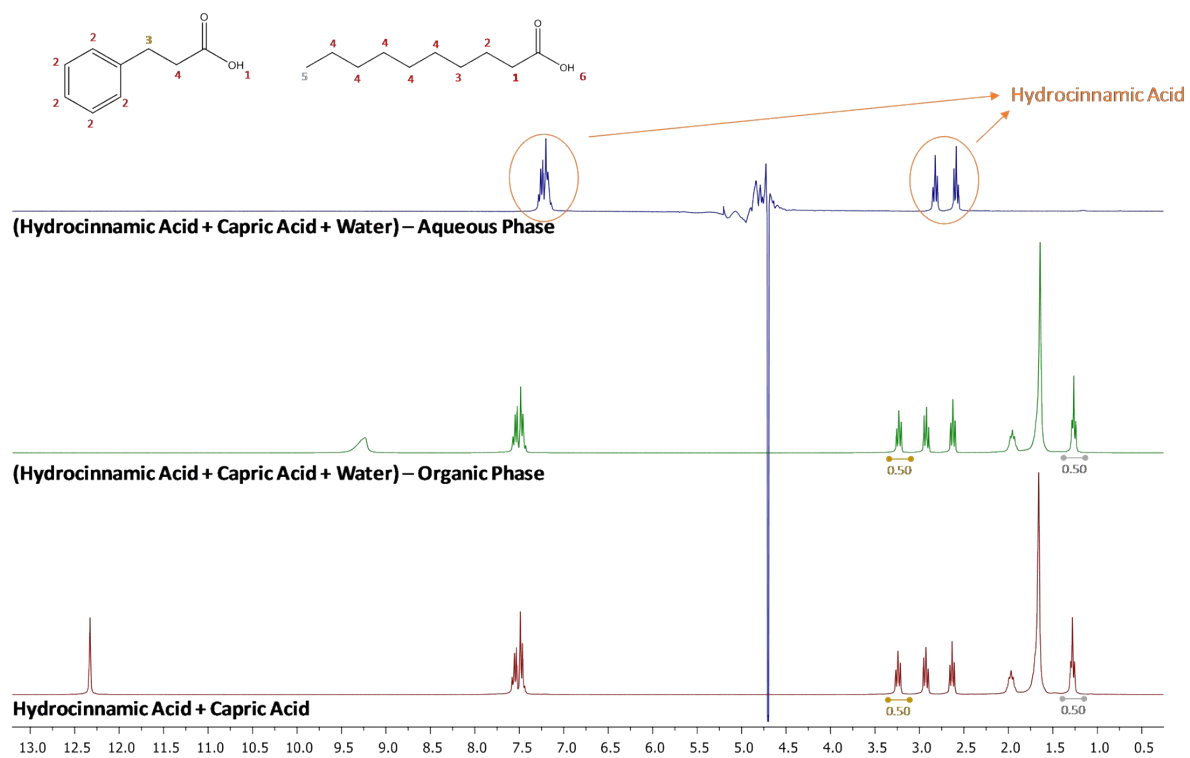
Figure S14. ^{1}H NMR spectra of HA+CA mixture (1:1) before and after contacting with deionized water for 24 hr at $T = 298$ K as well as the spectra of the aqueous phase after contact. All spectra were recorded at $T = 323$ K.
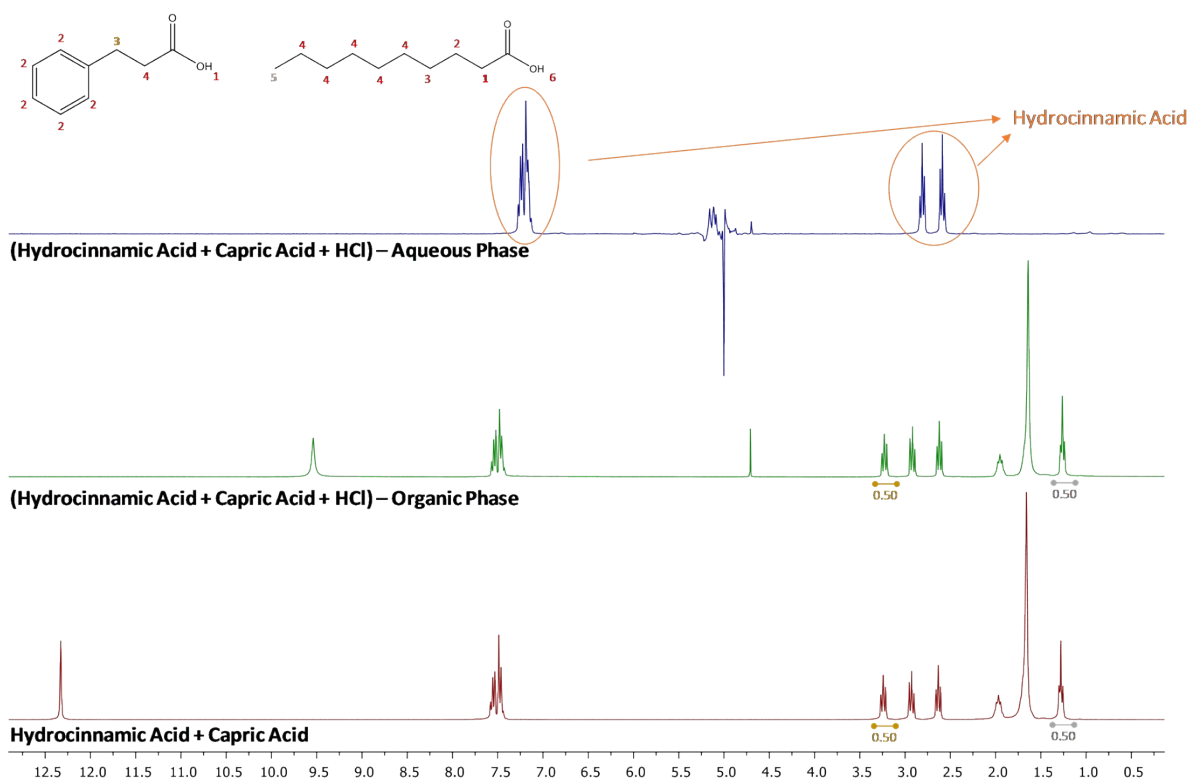
Figure S15. ^{1}H NMR spectra of HA+CA mixture (1:1) before and after contacting with an aqueous solution of 1 M HCl for 24 hr at $T = 298$ K as well as the spectra of the aqueous phase after contact. All spectra were recorded at $T = 323$ K.
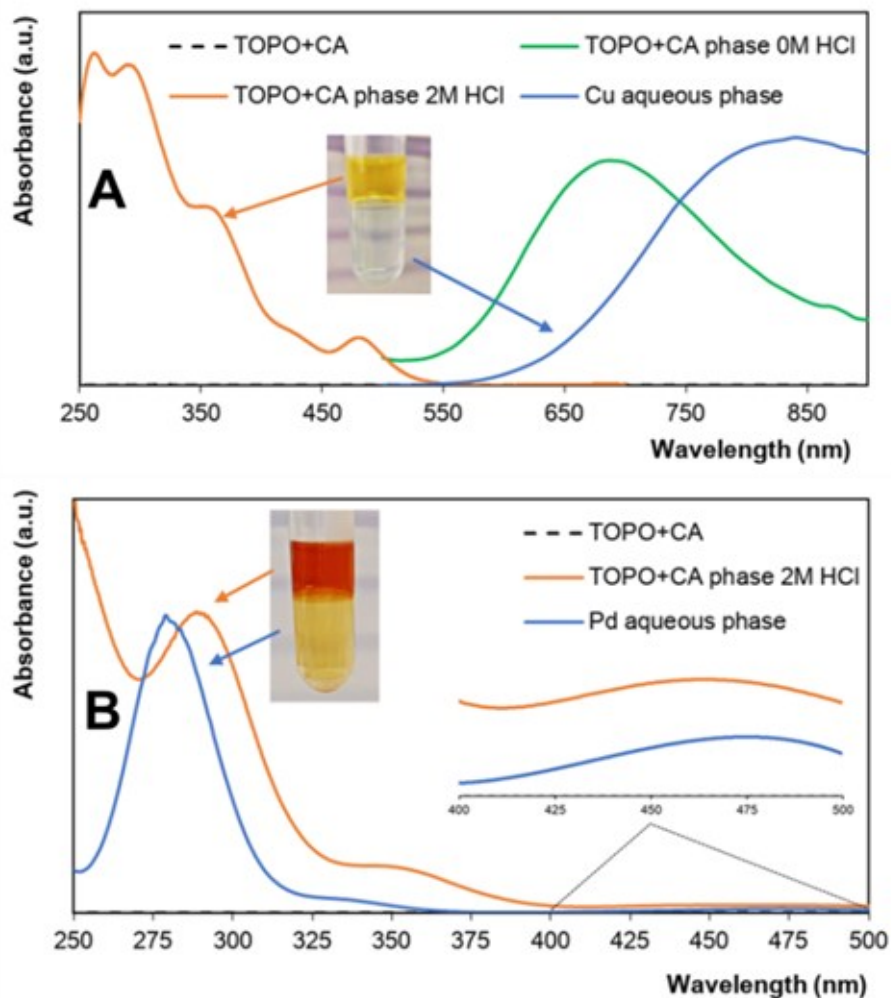
Figure S16. UV-vis spectra of the TOPO+Capric system (eutectic and aqueous phase) after extraction of A) 10 mM Cu^{2+} from H_2O and 2 M HCl solution and B) 10 mM Pd^{2+} from 2 M HCl solution. Band assignment panel A): $[Cu(H_2O)_6]^{2+}$ - 800 nm (blue), partially dehydrated copper carboxylate complex – 680 nm (green), $CuCl_4^{2-}$ - 291 nm and 415 nm (orange), $CuCl_2$ and $CuCl_3^-$ - 262 nm, 354 and 470 nm (orange).[16] Band assignment panel B): $PdCl_4^{2-}$ complex – 280nm and 478 nm (blue), neutral palladium complexes such as $Pd(OH)_2$ - 360 nm (orange).[17]
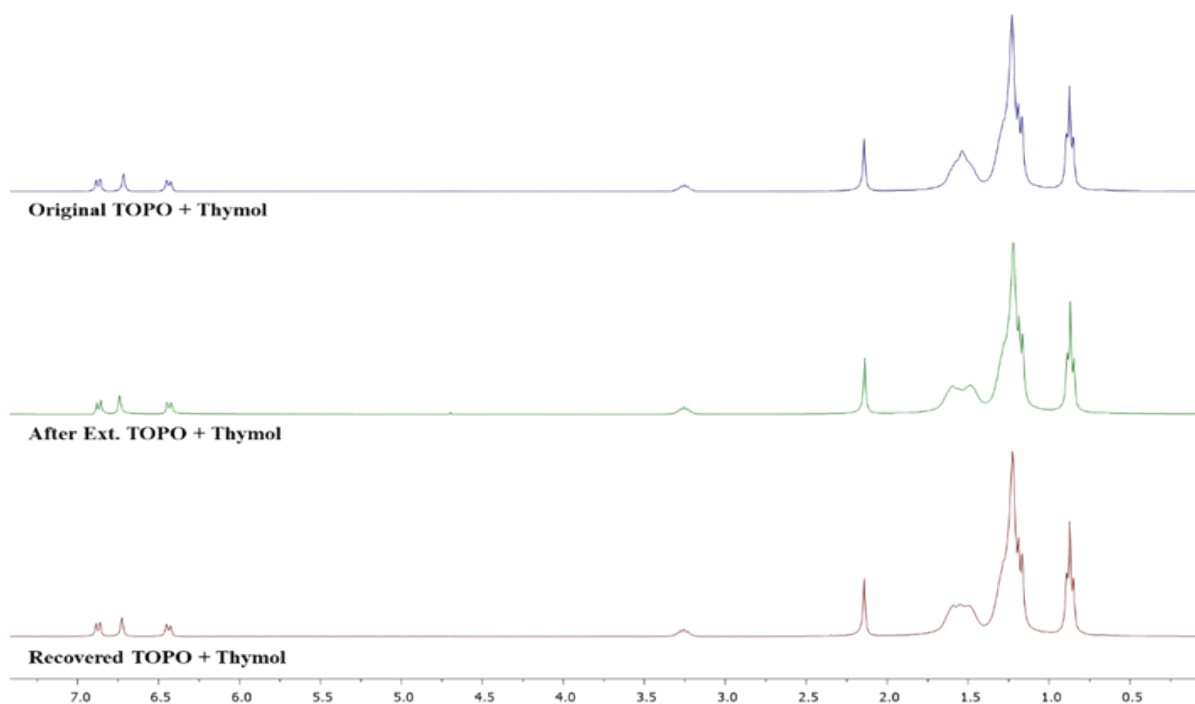
Figure S17. Experimental ^{1}H NMR spectrums of the Th+TOPO eutectic mixture before extraction (top), after extraction of 10 mM PdCl$_2$ from a 1 M HCl solution (middle) and after Pd^{2+} stripping using an acidic 0.1 M thiourea solution (bottom) at $T = 298$ K.
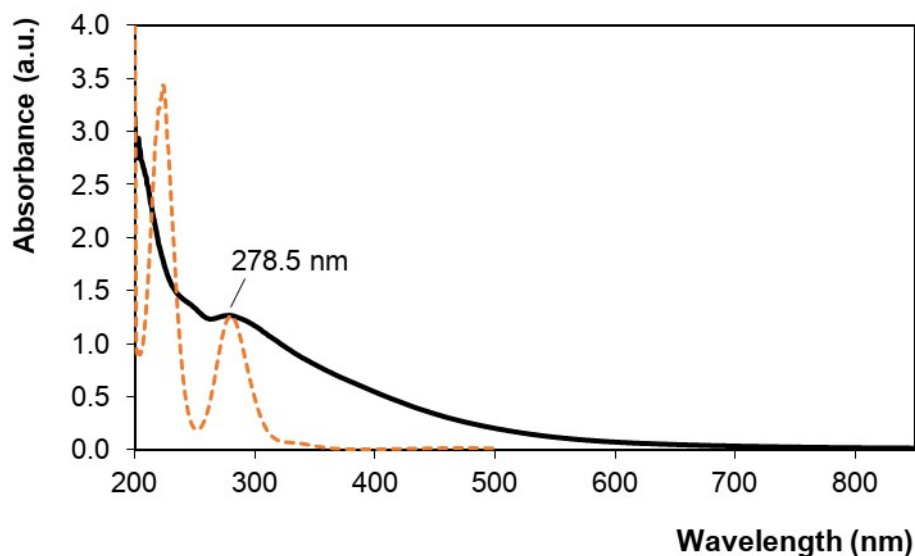
Figure S18. UV-vis spectra of the aqueous solution obtained from the loaded Th+TOPO phase after contacting with a 0.1 M NaCH$_3$COO (black line; contact time = 72 hr, O:A=0.5, x_{TOPO}= 0.5) compared to the spectra of PdCl$_2$ in 1 M HCl (orange dash).

Table S1. Summary of publications on the solvent extraction of metals using hydrophobic eutectic solvents.

HBD	HBA	HBD:HBA ratio	Studied metals ions	Separation potential	Ref
$C_nH_{2n}O_2$ (n=10, 12, 18), Ibuprofen (IBP)	$[N_{7,7,7,7}]Cl$, Menthol (M)	HBD+M - 1:2 HBD+$[N_{7777}]$Cl- 2:1 IBP+$[N_{7777}]$Cl - 3:7	In^{3+}	N.A.	[18]
$C_{10}H_{20}O_2$	Lidocaine	2:1, 3:1, 4:1	Co^{2+}, Ni^{2+}, Cu^{2+}, Zn^{2+}, Na^+, K^+, Li^+	M^{2+} from M^+	[19]
Phenol	$[N_{1,1,1,2(OH)}]Cl$	2:1, 3:1, 4:1	Co^{2+} with 1-nitroso-2-naphthol	N.A.	[20]
$C_nH_{2n}O_2$ (n=8, 10, 12, 14, 18)	Thymol (Th), Menthol (M)	$C_{10}H_{20}O_2$ + Th/M - full SLE studied Others - eutectic composition	Cu^{2+}, Zn^{2+}, Co^{2+}, Ni^{2+}, Mn^{2+}, Mg^{2+}, Ca^{2+}, Fe^{3+}, Cr^{3+}	Fe^{3+} and Cu^{2+} from others	[21]
Phenol	$C_{24}H_{51}PO$ (TOPO)	Full SLE studied	$[UO_2]^{2+}$	N.A.	[15]
$C_nH_{2n}O_2$ (n=6, 10)	$[P_{6,6,6,14}]Cl$, $[N_{8,8,8,8}]Br$	2:1	TcO_4^- in the presence of ReO_4^-, HCO_3^-, Cl^-, NO_3^-, $H_2PO_4^-$, I^-, SO_4^{2-}	N.A.	[22]
$C_{10}H_{20}O_2$	$[N_{4,4,4,4}]Cl$	2:1	CrO_4^{2-}, Cr^{3+}, Cu^{2+}, Ni^{2+}	$HCrO_4^-$ from others	[23]
$C_{10}H_{20}O_2$	$[N_{4,4,4,4}]Cl$	3:1	Ni^{2+} with sodium diethyldithiocarbamate	N.A.	[24]
Alkyl 4-hydroxybenzoate	$[N_{1,8,8,8}]Cl$	0.5:1 to 3:1	CrO_4^{2-} in the presence of Cd^{2+}, Cu^{2+}, Fe^{3+}	N.A.	[25]

Table S2. Properties of the chemical compounds used in the HES preparation.

Compounds	Abbr.	Supplier	CAS Number	M_w (g/mol)	Purity (%)	T_m (K)	ΔH_m (kJ/mol)	Solubility (g/L)
1-(2-pyridylazo)-2-naphthol	PAN	Sigma-Aldrich	85-85-8	249.27	Indicator grade	412.0[a]	-	0.000394 [34]
Acetylsalicylic Acid	Asp	TCI	50-78-2	180.16	> 98.0	407.4 [26]	23.01 [26]	4.600 [35]
Caffeine Anhydrous	Caff	Sigma	58-08-2	194.19	99.0	510.3 [26]	22.52 [26]	21.600 [35]
Capric Acid	CapAc	Acros Organics	334-48-5	172.26	99.0	304.8 [27]	27.50 [27]	0.0618 [35]
Coumarin	Cou	Sigma	91-64-5	146.14	99.0	343.0 [28]	18.63 [28]	2.494 [35]
Eugenol	Eu	Aldrich	97-53-0	164.20	99.0	269.2 [28]	18.72 [28]	2.46 [35]
trans-Ferulic Acid	tFerAc	TCI	537-98-4	194.18	99.0	444.9 [29]	30.50 [29]	5.970 [35]
Hydrocinnamic Acid	HydAc	Acros Organics	501-52-0	150.18	99.0	321.8 [30]	16.30 [30]	5.900 [35]
Mandelic Acid (L)	ManAc	Acros Organics	90-64-2/611-72-3	150.15	99.0	392.2 [31]	-	110 [35]
Salicylic Acid	SalAc	Acofarma	69-72-7	138.12	99.0	431.1 [28]	24.45 [28]	2.24 [35]
Syringic Acid	SyrAc	Acros Organics	530-57-4	198.17	> 97.0	480.3 [28]	33.70 [28]	-
Thymol	Thy	TCI	89-83-8	150.22	> 99.0	323.5 [32]	19.65 [32]	0.900 [35]
p-Toluenesulfonic Acid Monohydrated	p-TolAc	TCI	104-15-4	190.20	> 98.0	379.7 [33]	-	670 [36]
Trioctylphosphine oxide	TOPO	Aldrich	78-50-2	386.65	99.0	325.9[a]	58.02[a]	0.0015 [37]
Vanillic Acid	VanAc	Acros Organics	121-34-6	168.15	97.0	482.6 [26]	27.26 [26]	1.50 [35]

[a]Measured in this work by DSC.

Table S3. Absorption wavelengths used for the quantification of the studied metal ions by UV-vis.

Metal ion	Wavelength (nm)
Cobalt (II)	510
Copper (II)	800
Nickel (II)	395
Iron (III)	223, 334
Chromium (II)	413; 600
Palladium (II)	223, 280
Platinum (IV)	263

Table S4. Obtained hydrophobic eutectic solvents at 298 K.

Compound 1	Compound 2	Stoichiometry
Caffeine	Thymol	1:3
Acetylsalicylic Acid	Eugenol	
Coumarin	Thymol	
Eugenol	Thymol	
	Capric Acid	
	Coumarin	
Hydrocinnamic Acid	Thymol	
	Capric Acid	1:1
	Eugenol	
TOPO	Thymol	
	Capric Acid	
	Eugenol	
	Acetylsalicylic Acid	
	Hydrocinnamic Acid	

Table S5. System composition for the all-atom molecular dynamics simulations performed.

System	x_{TOPO}	Nº TOPO	Nº Thymol or Capric acid	Nº H_2O	Nº HCl	Box Type	Final Box Size (nm)
Th+TOPO	0.5	200	200	0	0	cubic	5.84^3
	0.4	160	240	0	0	cubic	5.65^3
	0.3	120	280	0	0	cubic	5.45^3
	0.2	80	320	0	0	cubic	5.24^3
TOPO+CA	0.5	200	200	0	0	cubic	5.95^3

Table S6. Experimental SLE data (x_2, T) and calculated activity coefficient (γ_i) for the systems measured in this work, at atmospheric pressure.

x_2	T / K	γ_1	x_2	T / K	γ_2
	Solid Phase: TOPO (1)			Solid Phase: Thymol (2)	
		TOPO + Thymol			
0.00	325.87[a]	1.00	0.70	260.00[a]	0.24
0.10	323.92[b]	0.98	0.80	276.24[a]	0.36
0.20	321.98[b]	0.97	0.90	312.55[a]	0.86
0.30	313.77[a]	0.62	1.00	323.50 [32]	1.00
0.40	303.33[a]	0.34			
0.50	279.62[a]	0.06			
0.60	264.87[a]	0.02			
	Solid Phase: TOPO (1)			Solid Phase: Capric Acid (2)	
		TOPO + Capric Acid			
0.00	325.87[a]	1.00	0.70	280.02[a]	0.55
0.10	324.65[b]	1.03	0.80	289.48[a]	0.70
0.20	322.90[b]	1.03	0.90	298.25[a]	0.88
0.30	313.78[a]	0.62	1.00	304.75 [32]	1.00
0.40	304.34[a]	0.37			
0.50	284.08[a]	0.09			
0.60	261.78[a]	0.01			
	Solid Phase: Hydrocinamic Acid (1)			Solid Phase: Capric Acid (2)	
		Hydrocinnamic Acid + Capric Acid			
0.00	321.16 [5]	1.00	0.60	288.09[a]	0.89
0.10	318.55[b]	1.06	0.70	293.17[a]	0.93
0.20	309.54[a]	1.00	0.80	296.38[a]	0.92
0.30	301.38[a]	0.97	0.90	300.44[a]	0.95
0.40	295.78[a]	1.01	1.00	304.75 [32]	1.00
0.45	291.47[a]	1.00			
0.50	288.65[a]	1.03			

[a]DSC, standard uncertainties, u, are $u(T_m) = 0.1$ K, $u_r(p) = 0.05$, $u_r(x) = 0.002$.

[b]Melting points device, standard uncertainties, u, are $u(T_m) = 1.2$ K, $u_r(p) = 0.05$, $u_r(x) = 0.002$.

Table S7. Experimental eutectic temperatures, T_e, of the systems investigated, measured using DSC[a].

x_2	T_e (K)	x_2	T_e (K)
TOPO + Capric Acid		**Hydrocinnamic Acid + Capric Acid**	
0.30	253.76 / 258.18	0.20	287.12
0.40	250.95 / 257.57	0.30	287.46
0.50	252.93 / 258.03	0.40	288.49
0.60	250.91 / 254.92	0.45	287.77
0.70	254.85	0.70	287.29
0.80	254.42	0.80	287.36
0.90	253.04	0.90	287.31

[a]DSC, standard uncertainties, u, are $u(T_m) = 0.1$ K, $u_r(p) = 0.05$, $u_r(x) = 0.002$.

Table S8. Distribution coefficient of metal ions as a function of HES selection and HCl concentration ($[Pt^{4+}]=[Pd^{2+}]=$ 2 mM; concentration of other metal ions was 10 mM; O:A=0.5; 1:1 HES molar composition). The HA+CA phase in the presence of Cr^{3+} (at 0 M HCl) emulsified and the concentration could not be measured.

Metal ion	0 M HCl			1 M HCl			2 M HCl		
	Th+TOPO	TOPO+CA	HA+CA	Th+TOPO	TOPO+CA	HA+CA	Th+TOPO	TOPO+CA	HA+CA
Pt^{4+}	16.62±0.13	16.92±0.56	0.04±0.02	182.2±4.03	259.1±14.5	0.63±0.01	327.6±12.3	830.2±52.1	0.63±0.03
Pd^{2+}	3.40±0.13	2.13±0.12	0.01±0.00	7.33±1.37	11.11±1.07	0.01±0.0'	18.16±2.31	25.04±0.90	0.18±0.03
Cu^{2+}	0.02±0.02	0.14±0.05	0.30±0.02	0.04±0.01	0.09±0.01	0.02±0.01	0.05±0.01	0.18±0.02	0.03±0.01
Co^{2+}	<0.01	0.03±0.01	0.13±0.01	<0.01	0.02±0.02	0.01±0.04	<0.01	0.22±0.04	0.13±0.02
Ni^{2+}	<0.01	<0.01±	<0.01	<0.01	<0.01	<0.01	<0.01	<0.01	<0.01
Cr^{3+}	0.09±0.01	0.16±0.02	Emulsion	<0.01	<0.01	<0.01	0.02±0.01	0.05±0.02	0.06±0.01
Fe^{3+}	0.08±0.02	1.17±0.11	26.68±1.10	4.81±0.04	8.16±0.24	0.04±0.04	280.7±38.9	1169±145	0.52±0.05

Table S9. Reported speciation of selected metallic ions with respect to chloride concentration. **Table S9** has to be considered as a qualitative summary of the possible species present but not their respective prevalence as the predicted speciation is known to change between studies and chloride source (HCl vs LiCl for example).

Metal ion	0.05 M Cl⁻	1.0 M Cl⁻	2.0 M Cl⁻
Pt(IV)[38]	$PtCl_4/PtCl_5^-/PtCl_6^{2-}$	$PtCl_6^{2-}$	$PtCl_6^{2-}$
Pd(II)[38]	$PdCl^+/PdCl_2/PdCl_3^-$	$PdCl_4^{2-}$	$PdCl_4^{2-}$
Cu(II)[39]	Cu^{2+}	$Cu^{2+}/CuCl^+$	$Cu^{2+}/CuCl^+/CuCl_2$
Co(II)[39]	Co^{2+}	Co^{2+}	Co^{2+}
Ni(II)[39]	Ni^{2+}	$Ni^{2+}/NiCl^+$	$Ni^{2+} / NiCl^+$
Cr(III)[40]	Cr^{3+}	$Cr^{3+}/CrCl^{2+}$	$Cr^{3+}/CrCl^{2+}/CrCl_2^+$
Fe(III)[41]	$Fe^{3+}/FeCl^{2+}$	$FeCl^{2+}/FeCl_2^+$	$FeCl^{2+}/FeCl_2^+/FeCl_3$

References

1 J.M. Prausnitz, R.N. Lichtenthaler, E.G. Azevedo, Molecular Thermodynamics Fluid Phase Equilibria; Prentice-Hall, 1986.

2 J. Gmehling, B. Kolbe, M. Kleiber, J. Rarey, Chemical Thermodynamics for Process Simulation; Wiley-VCH, 2012.

3 J.A.P. Coutinho, S.I. Andersen, E.H. Stenby, *Fluid Phase Equilib.*, 1995, **103**, 23-39.

4 M.J. Abraham, T. Murtola, R. Schulz, S. Páll, J.C. Smith, B. Hess, *Software X*, 2015, **1**, 19–25.

5 R. Hockney, S. Goel, J. Eastwood, *J. Comput. Phys.*, 1974, **14**, 148–158

6 H.J.C. Berendsen, H.R. Grigera, T.P. Straatsma, *J. Phys. Chem.*, 1987, **91**, 6269–6271.

7 B. Hess, H. Bekker, HJC Berendsen, J.G.E.M. Fraaije, *J. Comput. Chem.*, 1997, **18**, 1463–1472.

8 T. Darden, D. York, L. Pedersen, *J. Chem. Phys.*, 1993, **98**, 10089–10092.

9 D.J. Evans, B.L. Holian, *J. Chem. Phys.*, 1985, **83**, 4069–4074.

10 M. Parrinello, A. Rahman, *J. Appl. Phys.*, 1981, **52**, 7182–7190

11 W. Humphrey, A. Dalke, K. Schulten, *J. Mol. Graph.*, 1996, **14**, 33–38.

12 M.J. Frisch, et al., Gaussian 09 (revision D.01); Gaussian, Inc.: Wallingford, CT, USA, 2009.

13 Y. Zhao, D.G. Truhlar, D.G., *Theor. Chem. Acc.*, 2008, **120**, 215-241.

14 S.F. Boys, F. Bernardi, *Mol. Phys.*, 1970, **19**, 553-566.

15 M. Gilmore, E.N. McCourt, F. Connolly, P. Nockemann, M. Swadźba-Kwaśny, J.D. Holbrey, *ACS Sustainable Chem. Eng.*, 2018, **6**, 17323-17332

16 C. Amuli, M. Elleb, J. Meullemeestre, M.J. Schwing, F. Vierling, Inorg. Chem. 1986, 25, 856-861.

17 C. Drew Tait, D.R. Janecky, P.S.Z. Rogers, Geochim. Cosmochim. Acta, 1991, 55, 1253–1264.

18 E.E. Tereshatov, M.Y. Boltoeva, C.M. Folden III, C.M., *Green Chem.*, 2016, **18**, 4616-4622.

19 D.J.G.P. Van Osch, D. Parmentier, C.H.J.T. Dietz, A. van den Bruinhorst, R. Tuinier, M.C. Kroon, *Chem. Commun.,* 2016, **52**, 11987-11990.

20 M.B. Arain, E. Yilmaz, M. Soylak, M., *J. Mol. Liq.*, 2016, **224**, 538–543.

21 N. Schaeffer, M.A.R. Martins, C.M.S.S. Neves, S.P. Pinho, J.A.P. Coutinho, *Chem. Commun.*, 2018, **54**, 8104-8107.

22 T.E. Phelps, N. Bhawawet, S.S. Jurisson, G.A. Baker, *ACS Sustainable Chem. Eng.*, 2018, **611**, 13656-13661.

23 S. Ruggeri, F. Poletti, C. Zanardi, L. Pigani, B. Zanfrognini, E. Corsi, N. Dossi, M. Salomäki, H. Kivelä, J. Lukkari, F. Terzi, *Electrochim. Acta,* 2019, **295**, 124-129.

24 Z. Erbas, M. Soylak, E. Yilmaz, M. Dogan, *Microchem. J.*, 2019, 145, 745-750.

25 Y. Shi, D. Xiong, Y. Zhao, T. Li, K. Zhang, J. Fan, *Chemosphere*, 2020, **241**, 125082.

26 C. Su, Y. Chen, *Fluid Ph. Equilibria*, **2007**, 254, 167–173.

27 P.V.A. Pontes, E.A. Crespo, M.A.R. Martins, L.P. Silva, C.M.S.S. Neves, G.J. Maximo, M. Dupas Hubinger, E.A.C. Batista, S.P. Pinho, J.A.P. Coutinho, G. Sadowski, C. Held, *Fluid Ph. Equilibria*, 2017, **448**, 69-80.

28 U.S. Department of Commerce, NIST Chemistry WebBook, NIST Stand.

29 N. V. Shkaeva, D. S. Kosyakov, T. E. Skrebets, Y. N. Sazanov, *Russ. Chem. Bull.*, **2016**, 65, 2504–2508.

30 M. Iwahashi, S. Takebayashi, A. Umehara, Y. Kasahara, *Chem. Phys. Lipids*, **2004**, 129, 195–208.

31 PubChem, "Mandelic acid (Compound)." [Online,.Accessed: 05-Dec-2019].

32 M.A.R. Martins, E.A. Crespo, P.V.A. Pontes, L.P. Silva, M. Bülow, G.J. Maximo, E.A.C. Batista, C. Held, S.P. Pinho, J.A.P. Coutinho, *ACS Sustainable Chem. Eng.*, 2018, **6**, 8836–8846.

33 PubChem, "P-Toluenesulfonic acid." [Online,.Accessed: 05-Dec-2019].

34 L. Coo, T. J. Cardwell, R. W. Cattrall, S. D. Kolev, *Anal. Chim. Acta*, **1998**, 360, 153–159.

35 S.H. Yalkowsky S., Y. He, P. Jain, *Handbook of Aqueous Solubility Data*, 2nd ed. New York: Taylor and Francis Group, LLC, **2010**.

36 M. J. O'Neil, *The Merck Index: An Encyclopedia of Chemicals, Drugs, and Biologicals*, 1st ed. Cambridge: Royal Society of Chemistry, **2006**.

37 S. M. Elwaer, *Czechoslov. J. Phys*., **2003**, 53, A497–A499.

38 E. Högfeldt, IUPAC *Stability constants of metal-ion Complexes Part A: Inorganic ligands*; IUPAC; Pergamon Press, 1982.

39 R. Lommelen, T. Vander Hoogerstraete, B. Onghena, I. Billard, K. Binnemans, *Inorg. Chem*. **2019**, 58, 12289-12301.

40 M.J. Bjerrum, J. Bjerrum, *Acta Chem Scand*., **1990**, 44, 358–363.

41 W. Liu, B. Etschmann, J. Brugger, L. Spiccia, G. Foran, B. McInnes, *Chem. Geol*., **2006**, 231, 326-349.